A Biologically Inspired Soft Exosuit for Walking Assistance

Alan T. Asbeck[1,2] Stefano M. M. DeRossi[1,2] Kenneth G. Holt[3] Conor J. Walsh[1,2]

November 11, 2014

Abstract

We present the design and evaluation of a multi-articular soft exosuit that is portable, fully autonomous, and provides assistive torques to the wearer at the ankle and hip during walking. Traditional rigid exoskeletons can be challenging to perfectly align with a wearer's biological joints and can have large inertias, which can lead to the wearer altering their natural motion patterns. Exosuits, in comparison, use textiles to create tensile forces over the body in parallel with the muscles, enabling them to be light and not restrict the wearer's kinematics. We describe the biologically inspired design and function of our exosuit, including a simplified model of the suit's architecture and its interaction with the body. A key feature of the exosuit is that it can generate forces passively due to the body's motion, similar to the body's ligaments and tendons. These passively-generated forces can be supplemented by actively contracting Bowden cables using geared electric motors, to create peak forces in the suit of up to 200N. We define the suit-human series stiffness as an important parameter in the design of the exosuit and measure it on several subjects, and we perform human subjects testing to determine the biomechanical and physiological effects of the suit. Results from a five-subject study showed a minimal effect on gait kinematics and an average best-case metabolic reduction of 6.4%, comparing suit worn unpowered vs powered, during loaded walking with 34.6kg of carried mass including the exosuit and actuators (2.0kg on both legs, 10.1kg total).

1 Introduction

Robotic exoskeletons have been developed for a large number of applications, including assisting or enhancing human activities and rehabilitation. Some exoskeletons are stationary, mounted above treadmills and used to provide gait retraining or rehabilitation for those with disabilities or injuries (Banala et al, 2007; Jezernik et al, 2003; Veneman et al, 2007). Other exoskeletons are mobile, and these can be used to either support the full bodyweight of an individual or provide partial assistive torques. Devices in the former category are intended to be used by paralyzed individuals, enabling them to walk when they were previously unable to do so (Ackerman, 2010; Esquenazi et al, 2012; Neuhaus et al, 2011). In the latter category, exoskeletons providing partial gait assistance can either be used by disabled individuals for rehabilitation or gait augmentation, or by healthy individuals to improve strength or endurance. Several were designed exclusively for use by impaired individuals (Ohta et al, 2007; Quintero et al, 2011; Shorter et al, 2011), and these have been shown to improve walking speed or partially restore normal kinematics. Other systems were designed to augment healthy individuals, but these could also be used with impaired individuals for rehabilitation or assistance purposes, perhaps with modifications to their control strategies (Dollar and Herr, 2008; Herr, 2009). These include exoskeletons that aim to help people walk while expending less energy (Ferris and Lewis, 2009; Kawamoto et al, 2003; Pratt et al, 2004; Sawicki and Ferris, 2009a,b; Strausser and Kazerooni, 2011), and those that assist with heavy lifting (Wehner et al, 2009; Yamamoto et al, 2003). Still other exoskeletons assist healthy individuals with load carriage during walking by providing a parallel path to transfer load to the ground. These devices off-load the wearer, bypassing their musculature (Garcia et al, 2002; Kazerooni and Steger, 2006; Walsh et al, 2007). In this paper, we focus on the design of a system to augment healthy individuals during walking, but the same technology could potentially be used for rehabilitation or assistance to impaired individuals.

Assisting able-bodied individuals or patients with partial impairments poses particular challenges as an exoskeleton must be able to apply appropriate forces to the wearer yet not increase their metabolic expenditure. One mobile ankle exoskeleton (Mooney et al, 2014) has achieved a net metabolic reduction during walking at 1.5m/s with 23kg of load. Other devices thus far have only achieved a metabolic reduction for tethered or stationary activities. Two tethered devices have been shown to reduce the metabolic cost of walking, with one (Sawicki and Ferris, 2009b) showing a statistically significant reduction only at 1.75m/s out of several speeds tested, and another helping at 1.38m/s (Malcolm et al, 2013). For stationary activities, exoskeletons have been shown to reduce the wearer's metabolic effort for squatting (Gams et al,

[1]Harvard University, Cambridge, MA. aasbeck@gmail.com, walsh@seas.harvard.edu

[2]The Wyss Institute for Biologically Inspired Engineering, Cambridge, MA

[3]Boston University, Boston, MA.

2013) and hopping (Grabowski and Herr, 2009).

While our current system does not achieve this, our eventual goal is to build a portable soft wearable robot that is lightweight and low profile and that can reduce the net metabolic cost of walking. This task is difficult, however, because it is not yet clear if sufficient forces can be applied through a soft textile-based interface to provide sufficient benefit to offset the system mass that must be worn by the person. Furthermore, there are many other factors that can lead to a person's metabolic rate increasing while they are using a wearable robot; and so a successful device must provide beneficial torques while minimizing counterproductive effects. Many studies have evaluated the metabolic effects of adding assistance or mass to humans during walking; in the following paragraphs we review some of these results.

Humans are optimized to walk in a certain way, making use of the natural dynamics of the body and minimizing energy expenditure. If a system causes an individual to significantly alter their normal biomechanics, it will cause the wearer to expend additional energy (Gregorczyk et al, 2006; Walsh et al, 2007). In addition, the structure of the wearable robot can itself provide resistance to movement if the joints of a rigid system are misaligned with those of the wearer (Schiele and van der Helm, 2009). Specifically, Schiele (2009) reports that joint torques of up to 1.46Nm can be created due to joint misalignments that occur as an exoskeleton moves relative to the wearer over time, even if it was initially aligned correctly. These parasitic torques as well as constrained non-actuated degrees of freedom (DOF) can lead to deviation from the wearer's natural motion, discomfort, or injuries (Hidler and Wall, 2005; Pons, 2010; Schiele, 2009). Alternately, mechanisms aligning robotic and human joints can be complicated, increasing the mass of the exoskeleton (Cempini et al, 2013; Ergin and Patoglu, 2011; Schiele, 2009).

However, adding mass to the body raises its metabolic rate. Adding mass to the legs in particular changes their inertia which increases the metabolic cost of accelerating and decelerating them. The distribution of the mass is important as prior biomechanics studies have identified that mass at the foot during walking has a metabolic cost of 7.5-8.5% per kg of total added mass, as compared to 1-2% for mass at the waist (Browning et al, 2007; Rose and Gamble, 2006).

Finally, both humans and passive dynamic walkers use small amounts of input energy at specific times in the gait cycle during walking (Collins et al, 2005; McGeer, 1990). It has previously been shown that applying forces at the wrong time leads muscles to contract in order to compensate for the disturbance, which increases metabolic expenditure (Belanger and Patla, 1984; Tang et al, 1998). In addition, forces of randomly-varying magnitudes may be treated by the body as disturbances and lead to unwanted muscular contraction.

To summarize the preceding paragraphs, we understand that a metabolically-beneficial assistive device should maintain the normal biomechanics of walking; should minimize additional mass carried by the wearer, particularly on the distal portion of the leg; and should apply consistent small bursts of energy at the right time to the body. Looking to create a wearable robot that implements these features, we have recently proposed a new paradigm in assistive device design, namely soft clothing-like "exosuits" (Asbeck et al, 2013; Wehner et al, 2013). We define an exosuit as a wearable robot that does not contain any rigid elements that support compressive loads across the joints (Asbeck et al, 2013). Instead, the wearer's bone structure sustains all the compressive forces normally encountered by the body plus the forces generated by the suit.

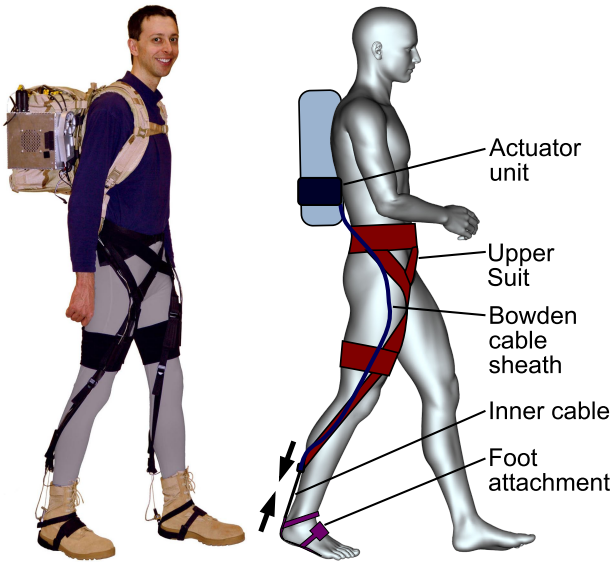

Figure 1: Left, picture of exosuit system. Right, diagram of exosuit system with components labeled. The actuator units are mounted on the outside of a backpack, which is empty except for the system's batteries. The upper suit is worn over the waist and legs. For each leg, an actuator unit powers a Bowden cable that extends down the leg and connects to the upper suit at the back of the calf. The inner cable extends downward from this point to the back of the heel, where it connects to a foot attachment. The arrows indicate the locations on the suit pulled together when the cable is actuated.

This paper describes the exosuit shown in Figure 1. Several other groups have previously proposed soft wearable robots intended to assist various joints in the legs during walking. Two of these robots are active soft orthotics that can provide slowly-varying forces to the ankle (Park et al, 2011) or ankle and knee (Stirling et al, 2011). Another device provides small amounts of hip flexion torque to induce the wearer to change their step length (Kawamura et al, 2013). Compared to these devices, our exosuit is portable, autonomous, lightweight, and has sufficient force-generating capability to apply biologically relevant torques to the joints of the wearer. Other researchers

have proposed exosuits to assist portions of the body besides the legs: one exosuit was designed to support the back during lifting tasks (Imamura et al, 2011; Tanaka et al, 2008), and another aids arm motions (Kobayashi, 2002). Two groups have developed exosuit gloves for assisting grasping and performing hand rehabilitation (In et al, 2011; Vanoglio et al, 2013).

When compared with traditional exoskeletons, exosuits offer a number of benefits. The suits themselves (composed primarily of fabrics), can be significantly lighter than exoskeleton frames or linkage systems. Thus, exosuits have comparatively lower inertias and thus metabolic cost associated with transporting the suit mass. Additionally, the wearer's kinematics are not restricted since a textile-based suit is flexible and can only apply tensile forces over the joints. Finally, exosuits are very low-profile, consisting primarily of a layer of fabric around the body, enabling them to be worn underneath regular clothing.

These benefits are important for applications requiring the system to be worn for long periods of time, such as hiking or load carriage, or for rehabilitation and assistance on an everyday basis. During loaded walking, a wearable robot that can reduce metabolic expenditure will delay the onset of fatigue, thus lowering the risk of injury by enabling individuals to maintain proper form for longer periods of time (Helbostad et al, 2007; Mizrahi et al, 2000; Pohl et al, 2010). In addition, such a system would reduce the loading on soft tissue (muscles, tendons, ligaments) that can be up to several times greater than those sustained in unloaded walking (Silder et al, 2013) thus reducing the risk of injury. For patients, such a system could perform two key and complementary functions: 1) provide small mechanical cues to assist with the initiation of movement and restore normal neuromuscular control, and 2) restore normal force-generating capability of the biological joints to improve walking efficiency. In this paper, we focus on assisting walking; however, the design concepts equally apply to other applications such as lifting tasks or using the upper body.

The fact that exosuits are not rigid and pull against the body presents a particular challenge in their design and operation, and presents a drawback when comparing them to rigid exoskeletons. In a traditional exoskeleton, it is assumed that if a motor or spring pulls on the exoskeleton frame, the frame will move as it is commanded, and the human will move with the frame. With a soft exosuit, however, the suit may displace considerably with respect to the compliant human underneath while applying high forces to the wearer. This can lead to a substantial amount of power being used to displace the exosuit as opposed to assisting the wearer, and a reduction in control bandwidth. Thus it is important to understand the stiffness properties of exosuit systems, to determine both their capabilities and how to design systems so the maximum power and force can be delivered to the wearer.

In this paper we present the design and evaluation of a soft exosuit that creates forces on the body during walking through a cable-actuated multi-articular textile that interfaces to the wearer at the pelvis, leg and foot. The architecture of the suit is such that it mimics the underlying function of the muscles at the hip and ankle and generates forces through a combination of passive and active tensioning. A diagram of the system is shown in Figure 1. It consists of one actuator unit per leg and the exosuit, which includes an upper suit, foot attachments, and a Bowden cable. To minimize mass along the legs, the actuator units are mounted on the wearer's torso (e.g. on a backpack) and each actuates one Bowden cable to transmit the force down the corresponding leg. The mass on both legs is only 2.0kg, including the suit (0.81kg) foot switches (0.44kg), and cables and force sensors (0.71kg). The total system mass is 10.1kg.

The upper suit is constructed from webbing and fabrics, and secures to the wearer's waist and thigh. On each leg, the bottom of it is connected to the sheath of the Bowden cable running down that leg, and the inner cable extends further and connects to the foot attachment. When the actuators retract the inner cable tension is created in the exosuit, which subsequently creates moments about the ankle and hip joints through the suit's architecture. We measure the force-deflection properties of the exosuit when it is on the wearer to characterize the series stiffness of the suit-human system. The system can create forces of up to 200N at the ankle, at walking speeds up to 1.5m/s (3.4mph), with a total power draw of 59.2W. Finally, we report the results of a number of walking trials where we evaluate the performance of the exosuit and its biomechanical and physiological effects on the wearer.

2 Biologically Inspired Design

2.1 Human Walking

The exosuit design is based on an understanding of the biomechanics of human walking. Humans expend much of the energy used during walking at gait transitions when the leg goes from the swing to stance phase and vice versa (Donelan et al, 2002). The leading leg absorbs energy when it contacts the ground, to cushion the collision and to store elastic energy in soft-tissues for subsequent rebound at push-off. The trailing (push-off) leg provides a small power burst as the lead foot hits the ground to transfer energy into the inverted body pendulum and to replace energy losses in the leading leg. The trailing leg also activates a small hip flexor muscle burst to initiate swing as the foot leaves the ground. From the perspective of the trailing leg, the preparation for pushoff, pushoff itself, and swing initiation take place between 30-60% in the gait cycle, defined as the time from one heel strike to the next for a given leg.

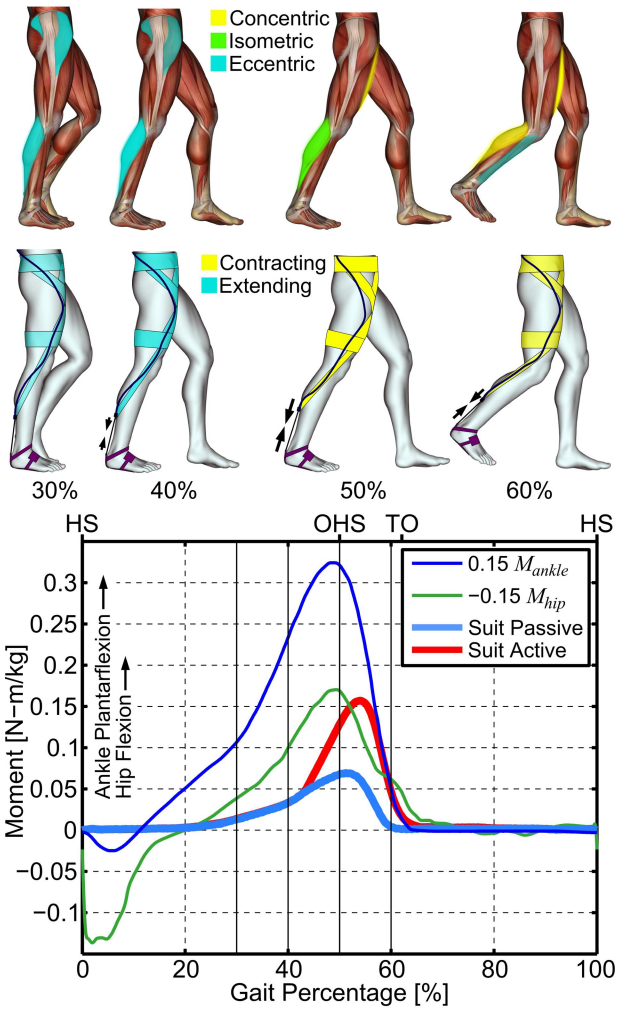

Figure 2: (a) Sequence of muscle activation during 30-60% in the gait cycle. The active muscles that are visible are highlighted, with the color indicating if the muscles are shortening (concentric contraction), holding a fixed length (isometric contraction), or lengthening (eccentric contraction) and the brightness indicating the magnitude of the muscle activity. (b) Diagrams of the exosuit over the same time period, during which forces are present in the suit. The color indicates if the suit is extending due to being stretched by the bodys motion, or contracting due to the cable retracting, and the size of the arrows at the heel indicates the magnitude of the force in the suit. (c) Plot showing the biological internal moments at the ankle and hip, scaled by 0.15, and with the hip moment inverted. Moments created by the suit at the ankle are also shown, including the moments if the suit is unactuated (Passive) or if is actively shortened (Active). Positive values on the graph correspond to ankle plantarflexion and hip flexion. Gait events are indicated at the top of the plot: HS=Heel strike, OHS=Opposite foot heel strike, TO=Toe-off.

The sequence of images in Figure 2(a) shows the activity of the relevant muscles during this phase of the gait cycle (Perry and Burnfield, 2010). At 30% in the gait cycle, the body's center of mass is near its peak over the extended leg, and it begins falling downward and forward. The calf muscles contract eccentrically during this time, passively elongating under the motion of the body falling forward. The Achilles' tendon also elongates as do the elastic elements in the muscle, absorbing some of the potential energy from the center of mass to be stored and later returned to the body for energy-efficient locomotion. This period of power absorption from the body continues until 40-45% in the gait cycle. Starting at this point, the stretched Achilles' tendon begins to rebound, returning some of the stored energy to the body, while the calf muscles contract isometrically, holding a constant length. Finally, starting at approximately 50-60% in the gait cycle, the calf muscles contract concentrically, shortening in length and providing additional power to complete the pushoff motion. At the hip, the ligaments holding the femur to the pelvis (not shown) and unactivated hip flexor muscles extend from 20-50% in the gait cycle, also absorbing power as the center of mass falls. The tensor fasciae latae muscle functions similarly, but also creating a hip abduction moment. The rectus femoris and other hip flexors then contract concentrically starting at 50-60% in the gait cycle, supplementing the power returned from the ligaments and pulling the leg forward to swing.

Looking at the plot in Figure 2(c), we see that the internal joint moments at the ankle and hip follow the activity of the muscles there. The ankle moment becomes positive (pushing the toe down into plantarflexion) at around 12% in the gait cycle, and increases as the body falls forward, lifting the heel until 50% of the gait cycle when the opposite leg touches down. The hip moment (here plotted negative from the typical convention, so that positive values correspond to pulling the hip into flexion) can be seen to be positive on the graph from 20-70% in the gait cycle. We observe that these moment curves are largely coincident in direction and magnitude, with small values at 20% in the gait cycle, peaking at 50% in the gait cycle, and returning to zero at 62-65% in the gait cycle.

2.2 Our Approach

Due to the near-symmetry of the moments at the ankle and hip, a multiarticular exosuit architecture can activate both of these joints simultaneously. Our system is designed to apply moments to the ankle and hip from 20-65% in the gait cycle, and be transparent to the wearer (i.e. apply zero forces) at other times. It is particularly important that the system be transparent during the swing phase of gait because the swinging leg acts like a pendulum (Doke et al, 2005), and external forces will disrupt the dynamics of that motion. As was mentioned, the exosuit extends from the waist to the heel, crossing both the ankle and hip

joints along the way. Moments are applied to each joint by positioning the suit on the correct side of the leg at each joint, and then creating a tension force in it at the appropriate times. This means that the suit must be located at the back of the ankle to create a plantarflexion moment, and at the front of the hip to create a flexion moment. We route the suit close to the center of the knee so it creates a minimal moment there, because the biological knee moment is small as compared to the ankle and hip moments (20% of the ankle moment, 40% of the hip moment). Furthermore, the knee moment switches direction from 40-60% in the gait cycle, making it complicated to design around. Our suit creates a slight knee flexion moment at 50-60% in the gait cycle, but this is small (15% of the ankle moment) and while beneficial will be ignored for the future discussion in this paper.

We choose to place the actuated cable across the ankle joint rather than elsewhere along the suit primarily because the ankle is the largest contributor to positive power during the walking cycle. By having the actuated region across the ankle joint, the ankle will receive the full force transmitted to the suit; the suit has slightly less tension across the hip due to friction with the skin along the leg. Furthermore, the ankle is narrower than the rest of the leg where the cable connects; this permits the cable to float above the skin in that region, preventing chafing during actuation.

Referring back to Figure 2, the second row of images shows the activity of the suit as compared to that of the muscles in the first row. A key aspect of how the suit works is that, as the cable is held at its initial position (its length at 0% in the gait cycle), the textile itself passively generates tension and absorbs power due to kinematic changes of the leg that cause the suit to stretch. This mirrors how the biological muscles contract isometrically, and the tendons and ligaments in the ankle and hip absorb power until 40% in the gait cycle. In the suit, after 43% in the gait cycle, the cable is actively shortened. This increases the tension force in it beyond what would naturally occur if the cable remained at its initial position, mimicking the concentric contraction of the muscles.

This behavior creates the suit moment profiles in the plot in Figure 2(c). The "Suit Passive" curve shows the induced moment at the ankle if the cable is held in a fixed position throughout the entire gait cycle. In this case, the suit elongates until just after 50% in the gait cycle, and then it returns to its original length, returning some of the absorbed energy. If additional energy is put into the suit by retracting the cable, then the induced moments are more than twice as large, as shown in the "Suit Active" curve. In this manner, the suit duplicates both the structure and function of the underlying muscles, tendons, and ligaments at the ankle and hip.

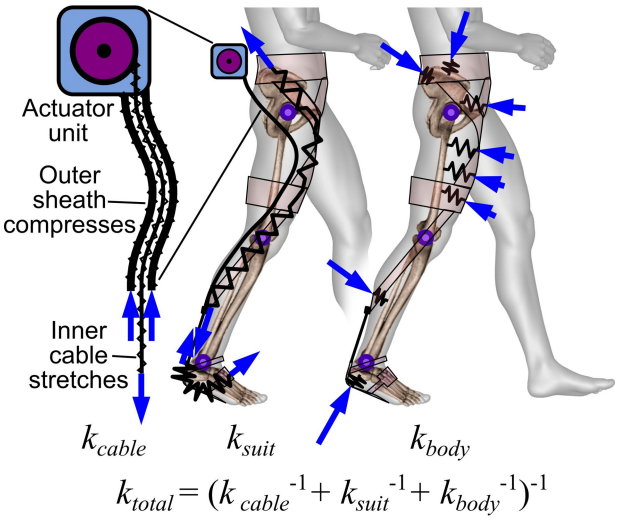

Figure 3: Sources of compliance in the suit-human system. The cable stiffness k_{cable} is due to the Bowden cable sheath compressing and the inner cable stretching. The suit stiffness k_{suit} is due to the fabric in the suit itself stretching. The body's stiffness k_{body} is due to the tissue between the suit and the bone compressing along the leg. The net stiffness k_{total} of the suit-human system is the series combination of these components.

2.3 Force production in the suit

There are two ways that force can be induced in the suit: the actuators can retract the Bowden cable, or the wearer can move. To understand either of these mechanisms, it is first necessary to understand the sources of compliance in the system. Figure 3 provides a lumped-parameter illustration of the suit and body, highlighting the main regions of compliance. In the Bowden cable itself, the outer sheath can compress and the inner cable can stretch. The textile material of the suit itself can stretch, and the soft tissue in the body can compress under the suit. The relationship between the force in the suit and the displacement along the length of the suit due to each of these three regions can be represented by a lumped stiffness, so they have stiffnesses k_{cable}, k_{suit}, and k_{body}, respectively. The series combination of these is k_{total}, which we refer to as the suit-human series stiffness.

If the wearer is stationary and the actuators retract the Bowden cables, force will be induced in the suit as a function of the actuator displacement due to the suit-human series stiffness. We measure k_{total} through this method as discussed in Section 3.2, and find that k_{total} is nonlinear in our system, with an actuator displacement of 6cm resulting in forces of 160N.

Force can also be induced in the suit if the wearer moves. The ability of the suit to passively generate tension due to the body's motion depends on its specific architecture, which we illustrate in Figure 4(a). The drawing at left defines the uncompressed body path length $s_{uncompressed}$, which is the distance along the surface of

the skin from the waist to the heel following the route that the suit takes over the top of the skin. We denote it "uncompressed" because it is the natural length of the skin without any tissue compression due to the suit. It includes a portion that extends from the waist to the front of the thigh (labeled s_1), a portion along the front of the thigh (s_2), and a portion which extends from just above the knee to the back of the foot (s_3), with total length s. Lengths $s1$ and $s3$ change as the wearer walks, because the angles of their hip, knee, and ankle vary over time.

If the suit is worn and the body compresses under the suit due to forces in the suit, we denote the new body path length as $s_{compressed}$, and the difference between these as

$$\Delta s = s_{uncompressed} - s_{compressed} \tag{1}$$

Another important length in the system is the unstretched suit length $l_{suit,unstretched}$, which extends from the heel to the waist. This is measured when no forces are applied to the suit, so the textile is unstretched. This is comprised of the initial textile length l_0 and the length of actuated cable at the back of the ankle, x_a, which can change over time as the actuators move:

$$l_{suit,unstretched} = l_0 + x_a \tag{2}$$

If forces are applied in the suit, it will stretch, resulting in a new length $l_{suit,stretched}$. We denote the change in suit length Δl, where

$$\Delta l = l_{suit,unstretched} - l_{suit,stretched} \tag{3}$$

We define x_{taut} as the difference between the unstretched suit length and the uncompressed body length:

$$x_{taut} = s_{uncompressed} - l_{suit,unstretched} \tag{4}$$

Values of x_{taut} less than zero correspond to slack in the suit, since the unstretched suit is longer than the uncompressed body path length. This is illustrated in Figure 4(a), which shows the leg at different times during the gait cycle. These drawings show the body path length $s_{uncompressed}$ as a black line, and the suit length $l_{suit,unstretched}$ on top of the body as a gray line, which is here assumed to remain at its initial length due the actuators staying in place ($x_a = x_{a,0}$). At certain times in the gait cycle, e.g. 0% and 80%, the suit will be slack because the suit length $l_{suit,unstretched}$ is longer than the body path length $s_{uncompressed}$. The drawing illustrates the slack by the gray suit length line reaching several centimeters away from the body at the hip and ankle.

At other times, e.g. 50% in the gait cycle, the uncompressed body path length grows to be longer than the unstretched suit length, so x_{taut} is positive. At these times,

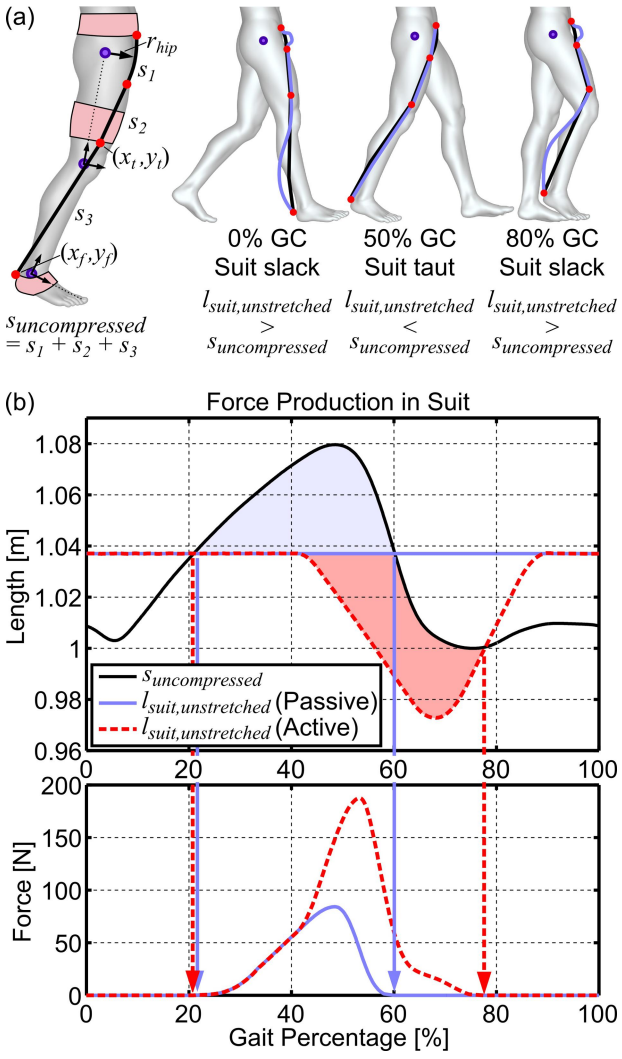

Figure 4: (a) Simple model of the uncompressed body path length $s_{uncompressed}$, which changes length during the gait cycle (GC). The model is composed of a segment around the hip that has a length proportional to the hip angle, a segment along the thigh which has a constant length, and a segment between the top of the knee and the heel that has a length which is a function of several distances and joint angles. In the right figures, $s_{uncompressed}$ is shown as a black line while the unstretched suit length $l_{suit,unstretched}$ is shown as a lighter line. (b) Top graph shows the uncompressed body path length $s_{uncompressed}$ as compared to two suit length conditions as a function of the percentage through the gait cycle for a sample individual. In one condition, the unstretched suit length held at its initial length ("Passive"), and in the other the unstretched suit length includes a portion where it is actively shortened ("Active"). As inputs to the body path length model, gait angles were used from (Perry and Burnfield, 2010) and the initial unstretched suit length was just under 1.04m, which is the distance from the bottom of the foot to the waist of a 180cm tall individual. Shaded areas indicate where the uncompressed body path length is longer than the unstretched suit length. This length discrepancy causes forces in the suit which are shown in the bottom graph.

the discrepancy in length must be resolved by one of several ways: either the kinematics of the person must change so that the uncompressed body path length remains small, the body must compress under the suit, the suit itself must stretch, or the Bowden inner cable must stretch and the sheath compress. The total displacement from these different sources must equal the length discrepancy x_{taut}. In practice, if the suit's stiffness is appropriately designed, the kinematics remain unchanged. This results in

$$x_{taut} = \Delta s + \Delta l \tag{5}$$

With this understanding, we can now define the suit-human series stiffness k_{total} as

$$k_{total} = \frac{d(\text{ Force in exosuit })}{d(x_{taut})} \tag{6}$$

The plots in Figure 4(b) illustrate the variation over time of the uncompressed body path length and unstretched suit length, and the subsequent force production in the suit. A simple model was created to estimate the lengths s_1 and s_3 over the course of the walking cycle; length s_2 remains constant. Length s_1 is assumed to vary as a function of the hip radius r_{hip} and the hip angle θ_{hip} with $s_1 = r_{hip}\theta_{hip}$. Length s_3 is a more complicated function of the knee and ankle joint angles, and the locations of the end of the strap with respect to the ankle and knee centers. The top end of the strap is a distance (x_t, y_t) above and to the front of the knee joint in a coordinate system with the y-axis extending upward from the knee joint to the hip joint. The bottom end of the strap is at a location (x_f, y_f) below and to the back of the ankle joint in a coordinate system with the x-axis parallel to the bottom of the foot. The strap is modeled as a straight line between these two points. In conjunction with joint angle data from (Perry and Burnfield, 2010), a very rough estimate of the uncompressed body path length $s_{uncompressed}$ can be computed as a function of the percentage through the gait cycle. In Figure 4, we use r_{hip} =8cm, $(x_t, y_t) = (3\text{cm}, 9\text{cm})$, and $(x_f, y_f) = (-8\text{cm}, -3\text{cm})$, and a distance of 44cm between the knee and ankle joints.

The uncompressed body path length is plotted in the top graph as the black line, reaching a peak at 48% in the gait cycle. The unstretched suit length $l_{suit,unstretched}$ is plotted as the gray horizontal solid line and is a constant value since it is held fixed at its initial value. Force is passively induced in the suit when the black line is above the gray line, which occurs from 20-60% in the gait cycle. This induced force is plotted as the gray solid curve in the lower graph in Figure 4(b).

This passively-induced force profile has a peak value of 80N in this example. This particular value of the peak force is a function of the suit-human series stiffness and the initial unstretched suit length. If the initial suit length was longer, for example, then the length discrepancy x_{taut} between the body's uncompressed path and the suit's unstretched length would be smaller, resulting in reduced forces in the suit and the profile having a slightly different shape. In practice, the initial unstretched suit length can be adjusted readily by using the actuators to retract or extend cable, thus changing x_a.

In addition to the suit/tissue absorbing and returning power passively, energy can be added through actively retracting the cable with the actuator units during the walking cycle. This has the effect of shortening the unstretched suit length: in Figure 4, the dashed line shows the unstretched suit length shortened from 40-86% in the gait cycle, and held at its initial value otherwise. This new, time-varying unstretched suit length is less than the uncompressed body path length $s_{uncompressed}$ from 20-77% in the gait cycle, and so the induced force is positive during this time as well. Furthermore, the difference in length x_{taut} is now greater than it was in the passive condition, and so the induced force in the suit is greater in magnitude as well.

To operate the suit in practice, we choose a desired peak passive force (e.g. 50N or 80N) and a desired peak active force (e.g. 100N, 150N, or 200N) as these values were found to be comfortable for subjects during walking trials. The initial unstretched suit length is determined by a wearer donning the suit, walking with the suit in passive mode, and observing the forces at the ankle. The length of the suit is then gradually adjusted through shortening or lengthening the cable until the peak forces in the suit match the desired passive value. This is done for each leg separately to make sure the suit is set up symmetrically. After the initial unstretched suit length is set by this method, actuation is applied, which will result in a new peak force. Keeping the initial suit length constant, the actuation pull amplitude is then adjusted for both legs together until the peak observed forces match the desired peak active force.

Finally, the suit can be made to be completely transparent to the wearer at any point in the gait cycle by lengthening the cable so the suit is slack, at which point it feels much like wearing a pair of pants.

3 Exosuit Design and Characterization

We next discuss specifications we followed in designing the exosuit, present its construction in detail, and provide results from testing the suit-human series stiffness.

3.1 Suit Specifications, Construction, and Force Transfer

3.1.1 Specifications

We followed a number of principles in designing the suit in an attempt to maximize the suit's comfort and the power transfer to the wearer, as previously described in (Asbeck et al, 2013). Related design principles are explained in (Kang et al, 2012) for a robotic exoglove.

1. Maximize suit-human series stiffness in order to maximize power transfer to the human
When the suit is actuated, the cable's displacement is in series with the suit-human series stiffness k_{total}, similar to a series elastic actuator (SEA). There are two main differences between the exosuit-human system and a traditional SEA. First, the exosuit-human system is nonlinear and hysteretic, which is characterized further in Section 3.2. Second, the suit-human series stiffness is quite low as compared to most SEAs. Hollander et al. did analysis of different spring stiffnesses for a powered ankle assistive device based on an SEA (Hollander and Sugar, 2007; Hollander et al, 2006). They found that low spring stiffnesses below 20,278 N/m (with a moment arm of 12cm) result in a high energy cost for the system because most of the energy goes into stretching the spring instead of causing the joint to move. Thus, to minimize the power usage of the system, the suit-human series stiffness should be increased above its own critical point. Furthermore, if the suit-human series stiffness is increased to a very high value, a secondary spring with very low hysteresis can be placed in series with it. This will decrease the overall hysteresis of the exosuit, a desirable effect, and will reduce the suit-human series stiffness to some desired value. We used the following guidelines in an attempt to design a suit that maximized the suit-human series stiffness:

- ***Anchor the suit to locations on the body that have high stiffness.***
  The suit is in series with its anchoring points, so the system is only as stiff as these locations. In general, the direction normal to the body will be stiffer than the direction tangent to the skin because underlying bones are rigid and will resist deformation.
- ***Choose suit materials with as high of a stiffness as possible.***
  The textiles comprising the suit can stretch (k_{suit} in Figure 3), which will reduce the suit-human series stiffness.
- ***Follow the most direct paths for transferring force across the body.***
  Routing the tensile paths in the suit in the most direct manner possible from one point to another will reduce the required tension in the elements, reducing forces on the anchoring points as well as minimizing deflection.

2. Maximize comfort for the wearer.
For the system to be able to worn for long periods of time, it must be comfortable. To maximize comfort, we designed the suit to:

- ***Minimize shear forces between the suit and human.***
  Shear forces on the skin are known to be uncomfortable (Cool, 1989), and may lead to chafing if there is motion of the suit relative to the skin. Even if the suit does not move relative to the skin, the skin can move relative to the underlying bone structure which may lower suit stiffness. In general, shear forces between the suit and human can be minimized by choosing careful suit force paths and maximizing the suit-human series stiffness. This will lead in turn to lower suit displacements for a given force in the suit and thus lower shear stress between the suit and human.
- ***Maximize the suit-skin contact area to minimize normal pressure and maximize stiffness.***
  Increasing the contact area between the suit and skin helps maximize the suit-human series stiffness both through reducing pressure ($Pressure = Force/Area$) and also reducing suit deflection (lower pressure leads to lower deflection per unit area in the normal direction). Several studies have indicated that steady-state normal pressures on the skin above 0.5N/cm^2 result in discomfort and restricted blood flow (Cool, 1989; Holloway et al, 1976).

3.1.2 Suit Construction

The specific suit discussed and evaluated in this paper is shown in Figure 5. The upper suit is composed of a waist belt (1), thigh braces (6), and connecting straps (2-5,7,8). The Bowden cable sheath attaches distally to the exosuit at (9) as well as being secured to the suit at the knee and thigh to hold it near the leg. The suit incorporates adjustability with buckles and Velcro so the various elements can be positioned precisely with respect to biological landmarks for wearers with height in the range of 1.68-2.0 meters. The suit utilizes relatively inextensible seatbelt webbing so the textile itself has high stiffness and low hysteresis, and uses a type of Velcro with short hooks and a low pile loop (Velcro-brand 845 Hook, 3610 Loop) to reduce the deflection at the suit adjustment points. Except at the back of the calf, 2" wide webbing is used along the leg in order to maximize the suit-human contact area.

The waist belt consists of two 1" polyester webbing straps, positioned above and below the wearer's iliac crest, with ripstop nylon fabric in between. Strap 5 intersects the waist belt over the wearer's iliac crest, and a small (4cm x 5cm) piece of foam is located there to distribute the pressure over the bone. Strap 2 connects to the waist belt below the iliac crest and is supported by the bony region at the lower back of the pelvis. The waist belt also has a foam pad that cushions the lower back.

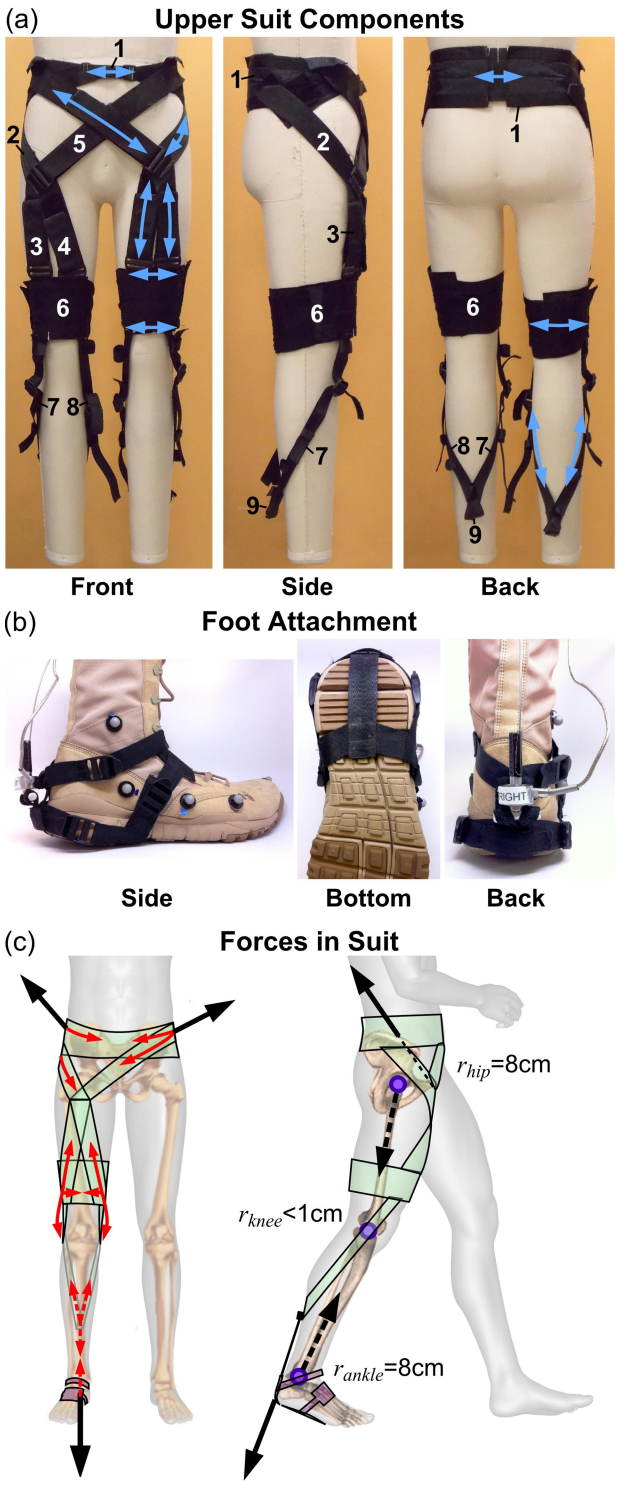

Figure 5: (a) Views of the upper suit with components labeled. Arrows indicate places where it can be adjusted to fit different sizes of individual. (b) Views of the foot attachment. (c) Forces in the exosuit and radii around the ankle, knee, and hip which are the distance between the biological joint and the force path in the exosuit. Large solid arrows are the net forces on the suit due to the body at the pelvis and heel. Small arrows (left side) show the paths transferring that force within the suit. Large dashed arrows (right side) show the reaction forces on the hip and ankle joints compressing the skeletal structure.

Straps 2 and 5 come together at the "thigh node" in the center of the thigh just below the crease of the leg. This junction must be positioned precisely in the center of the leg, since the remainder of the suit hangs from it. If it is incorrectly aligned (to one side), the suit below that point will rotate in that direction over time as it is actuated. Also, the intersection of straps 5 from the right and left legs was chosen to be above the height of the hip joint so as to not restrict motion of the legs in the frontal plane.

From the thigh node, straps 3 and 4 extend to both sides of the leg symmetrically, and are connected to straps 7 and 8 which extend down to the back of the calf. The thigh brace 6 permits the distance between the bottom of straps 3 and 4, and the tops of straps 7 and 8 to be adjusted, so that straps 7 and 8 can be positioned properly as they pass through the knee. Typically, both straps 7 and 8 are positioned slightly in front of the knee, so their back edge passes through the center of rotation of the knee if the wearer is standing vertically. When the wearer has their leg back, the straps migrate so that their centers pass through the knee's center of rotation. When the wearer bends their knee, they both move behind the knee, with the outer strap usually moving further than the inner strap due to the geometry of the leg muscles. Straps 7 and 8 are adjusted so the connection point to the Bowden cable sheath, 9, is in the center of the leg.

The foot attachments (Figure 5(b)) are constructed of 3/4" and 1" nylon webbing which is adjustable with buckles and secured with Velcro. Straps extend from the back of the heel under the boot and to the top of the foot, where a wide patch distributes the pressure. Additional straps around the ankle and around the sides of the heel serve to hold the foot attachment in place. The foot attachments were designed to be compatible with military boots, which were worn by all subjects during testing.

3.1.3 Force Path Routing in the Suit

The suit architecture creates forces in the suit as shown in Figure 5(c) as the webbing routes transfer force from the foot to the waist. The final architecture was determined by following the general guidelines in Section 3.1.1 and by experimenting with different strap placements to improve the suit's comfort and the suit-human series stiffness.

At the waist, the suit is anchored to the pelvis bone, which supports the majority of the downward force in the system (some shear force is supported by the skin along the leg). The pelvis was chosen as an anchoring region since it has high stiffness, with much of the bone covered only by a thin layer of tissue. Strap 5 transmits the majority of its force to the corner of the iliac crest, and strap 2 transmits its force to the back of the pelvis. These straps were routed in this manner in order to transmit the force down the leg the most directly and to minimize shear forces on the skin.

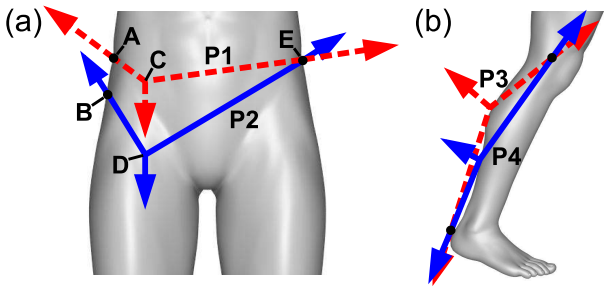

Figure 6: (a) Two possible paths for the straps around the waist. Path P2 (solid lines) has lower displacement in the middle and lower forces at the hips than path P1 (dashed lines) for a given downward force at point D or C, respectively. Arrows indicate the forces on the ends of that segment of the suit: arrows at the hip are forces due to the body, and forces at the thigh are due to the lower connecting portion of the suit. (b) Two possible paths for the straps between the knee and the heel. Path P4 is more direct and will press into the calf less than path P3, resulting in less displacement at the heel and higher comfort for the wearer. Large arrows again indicate forces on that portion of the suit, due to (from top to bottom) the rest of the suit above the knee, the calf pushing out on the strap, or the foot attachment pulling the bottom of the strap down.

Figure 6(a) shows two different possible paths we examined for straps 2 and 5. If the junction where these meet is high on the leg, as with path P1, large inward forces are created at the sides of the pelvis when a vertical force is applied at point C. This point also experienced large amounts of downward deflection due to the shallow angles to the sides of the body, leading to a small stiffness in the vertical direction.

An alternate path that was also found to not work well was between the points A, D, and E in Figure 6(a). In this path, the angle of strap 2 (between A and D) is quite vertical, which led to significant shear forces on the point where it contacted the pelvis. In early prototypes we tested, this strap placement was found to lead to the strap moving downwards over the iliac crest during suit actuation, which led to a low suit-human series stiffness and discomfort for the wearer.

Instead, we used the strap routing P2, which passes around the side of the pelvis. There, it is able to apply a force much more substantially in the normal direction (force 56° from parallel to the skin as opposed to 34°), leading to increased comfort and an increased suit-human series stiffness.

Further down the leg, another example of routing the straps directly to achieve higher suit-human series stiffness is the path of straps 7 and 8 at the back of the calf, shown in Figure 6(b). These straps were routed below the bulk of the calf muscle, following path P4. For comparison, the straps in Path P3 have a larger change in angle as they bend around the calf which results in a larger normal force vector on the calf. This leads to a larger inward displacement into the calf muscle, which causes the lower end of the straps to displace downward more, thereby reducing the suit-human series stiffness.

Finally, the suit anchored to the bottom of the foot, another region able to resist normal loads with high stiffness. In summary, the force paths throughout the suit were chosen in order to maximize the suit's comfort and the suit-human series stiffness. Ongoing work is focusing on the optimization of these force transmission paths to maximize the suit-human series stiffness while ensuring comfort for the wearer.

3.2 Suit-Human Series Stiffness Measurements

In order to understand the behavior of the suit-human system, it is necessary to characterize the suit-human series stiffness. Understanding this permits accurate calculations for the required actuator speeds and power consumption. We performed studies of the suit-human series stiffness for $N = 6$ subjects, who were all approximately the same height (179.7cm−190.5cm, Avg= 184.8cm, Std= 4.69cm) but with varying weights (74.7kg−105.2kg, Avg= 87.5kg, Std= 9.85kg). Subjects gave informed consent and testing was approved by the Harvard Institutional Review Board (IRB).

To characterize the suit-human series stiffness k_{total}, subjects stood in a pose similar to that in which the suit is actuated during walking, with one heel 50cm in front of the other (shown in the inset in Figure 7). The cable was then actuated in a ramp profile with amplitude 8cm (0.52 seconds up, 2.5 seconds pause, 0.52 seconds down, 1.0 seconds pause, repeat) while recording the motor position and the induced force in the suit. Since the wearer stood stationary, the length discrepancy x_{taut} between the uncompressed body path length and the unstretched suit length was due solely to the actuator's motion. The measured displacement includes components from the foot attachment, the exosuit and human (which includes the suit material stretching and the underlying tissue deforming), and the cable.

Figure 7 shows the results of force in the suit versus cable position at the actuator output. Results from the 6 subjects are shown in thin lines, and curves fitted to the average across subjects are in thicker lines. The force-displacement curve has hysteresis, and arrows indicate the direction of travel around the loop. To fit equations, the hysteresis loop was divided up into four regions, I-IV. The rising curve was fitted to polynomials in regions I and II, and the falling curve was fitted with an exponential in region III and a flat line in region IV. The equations of fit are:

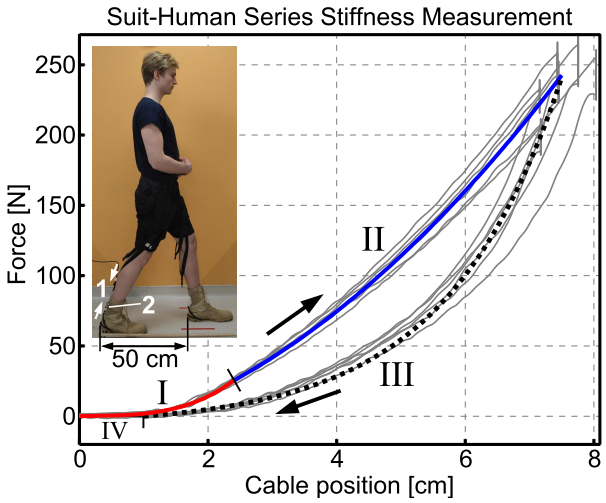

Figure 7: Force in suit vs. cable position. Testing results for 6 subjects are shown in thin lines, and lines of best fit to the group are shown in thicker lines. Different regions I-IV are separated by small perpendicular lines, and contain different lines of best fit. Arrows indicate the direction of the hysteresis loop. Subjects stood in the pose shown in the inset, with their heels separated by 50cm. The cable position was shortened at (1), and the force measured at (2).

Rising curve:

$$\text{I: } F = 2.457x^3 - 2.107x^2 + 1.481x \qquad x <= 2.4019$$

$$\text{II: } F = 3.385x^2 + 9.065x - 15.849 \qquad 2.4019 < x <= 7.518$$

Falling curve:

$$\text{III: } F = 6.5(exp(0.56(x-1)) - 1) \qquad 1 < x <= 7.518$$

$$\text{IV: } F = 0 \qquad x <= 1$$

where x is in centimeters and F is in Newtons. For arbitrary values (x_p, F_p) of the peak displacement and force of the rising curve, the falling curve is scaled to be:

Scaled Falling curve:

$$\text{III: } F = A\ 6.5(exp(c\ 0.56(x-1)) - 1) \qquad 1 < x <= x_p$$

$$\text{IV: } F = 0 \qquad x <= 1$$

where

$$A = \frac{F_p}{F^*} \qquad \text{and}$$

$$c = \frac{x_p - 1}{x^* - 1}$$

with $(x^*, F^*) = (7.518, 243.6)$. These equations are used to model the suit's behavior in later experiments (Section 4.3.2), and are also used to generate the force simulation plot in Figure 4. The rising curve is fitted by a cubic equation for small displacements and by a quadratic equation for larger displacements, which means the suit-human series stiffness increases quadratically and linearly with displacement, respectively. Even at large displacements, the resulting stiffness is still several times smaller than the ideal spring stiffnesses for actuating the ankle (Hollander and Sugar, 2007; Hollander et al, 2006).

The hysteresis in the load-unload cycles results in a loss of energy for every cycle. The suit returned approximately 64.9% of the energy in each cycle. This is small compared to the energy returned by tendons (90-93%) (Finni et al, 2013; Shadwick, 1990), which means that energy must be added to the suit as it relaxes to duplicate the behavior of muscles and tendons.

4 Actuation, Control, and Power Transfer

4.1 Actuation

Two actuator units are used to retract the Bowden cables (Nokon brand bicycle brake cables) during walking. A schematic illustrating the actuation scheme is shown in Figure 8. Each actuator unit contains a geared motor (Maxon EC 4pole 30, 200W, 24V with a 111:1 gearbox) which wraps up the inner cable of the Bowden cable around a pulley (radius = 3.5cm). The force on the cable at the top of the Bowden cable was measured via a cantilevered load cell (Phidgets 3135 50kg Micro Load Cell) with an idler pulley on its end. With the inner cable passing over the idler, tension in the cable causes the cantilever to deflect slightly, which is detected by the load cell. A second load cell (Futek LCM300) is positioned at the ankle, in series with the cable, to measure the true forces delivered to the wearer.

4.2 Control system

We used a simplistic control scheme as a proof-of-concept to evaluate the exosuit's performance during steady-state walking. Foot switches (B&L Engineering) are worn to detect heel strike, which show a rise in their signal within 0.01 seconds after the true heel strike as detected by a force plate. The control scheme was then executed with a realtime control loop at 1 kHz using the Matlab xPC

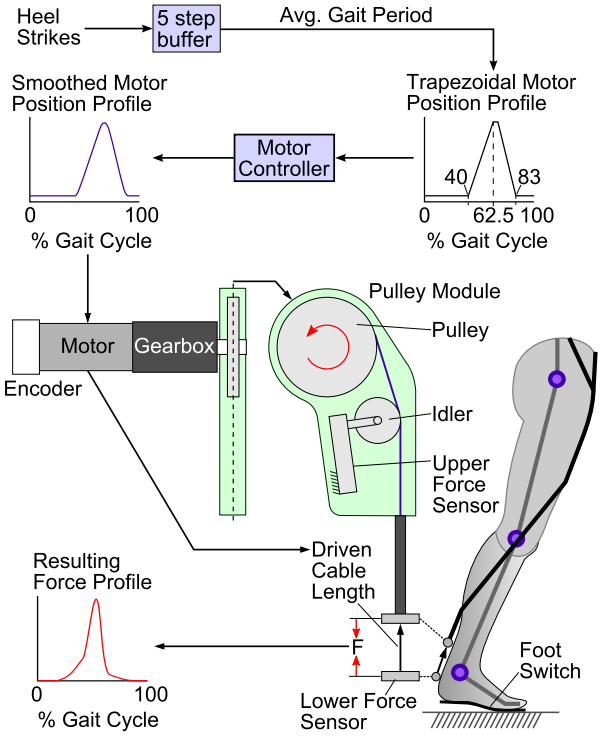

Figure 8: Diagram of the actuation scheme. Heel strikes are detected with foot switches, and the average gait period is computed using the previous five heel strikes. Using this average gait period, a trapezoidal motor position profile is computed based on the estimated percentage through the gait cycle at each point in time. This is sent to the motor controller, which computes a velocity- and acceleration-limited version that is sent to the motor. This position profile is the driven cable length, where positive values correspond to retracting the cable. This cable displacement induces a force in the suit through the suit-human series stiffness, which is monitored with a load cell at the ankle but not used for feedback. Mechanically, a geared motor drives a circular pulley which winds up the cable around it as it rotates. After unwrapping from the pulley, the cable passes over an idler pulley connected to a cantilever-style load cell. The cable changes angle over the idler, causing a force on the idler when there is tension in the cable, and thus enabling the tension in the cable to be measured. The Bowden cable sheath is attached to the bottom of this pulley module, and the inner cable remains inside the sheath until it reaches the ankle.

Target operating system on a PC/104 computer (Diamond Systems). The system stores a buffer of the past five heel strike times, which are used to compute the average gait period. Following a foot strike, the system executes a position-controlled motor trajectory as a function of the current estimated percentage through the gait cycle (as estimated by the average foot strike period and time since the most recent heel strike). The PC/104 computes a trapezoidal profile, which is sent to a Copley Accelnet ADP-090-36 motor controller that controls the position of the motor so it follows this trajectory (subject to a motor acceleration limit of 2500 rotations/sec^2). This flow of signals is shown in Figure 8. Signals are logged at 200 Hz. The control scheme described here is intended for situations in which the wearer varies their cadence and walking speed slowly; many further improvements would be needed for a general over-ground walking system.

For our set of initial walking experiments, the trapezoid was set to begin at 40% in the gait cycle, have the beginning of the plateau at 62.5% in the gait cycle, and return to the starting position at 83% in the gait cycle. The point at which the trapezoid began decreasing varied depending on the pulse amplitude. Using a maximum motor velocity of 11500 rpm, the end point of the plateau in the trapezoid was calculated based on a linear decrease at this speed and finishing at 83% in the gait cycle. This resulted in slightly varying motor profiles when smoothed by the motor controller. This particular motor profile was selected based on feedback from people wearing the system and was simple to compute.

The Bowden cables have friction that varies over time as they wear out ($\sim$70% efficiency dropping to $\sim$50% efficiency), and the friction also varies as a function of the leg's configuration during walking. A position-controlled cable trajectory was thus selected as it is immune to varying friction, while open-loop force-based methods will change characteristics over time. In addition, the bandwidth of the system presented here was too slow to do closed-loop force control using the ankle force sensor as feedback. Finally, because the suit-human stiffness behavior is very consistent across subjects and between days, a motor position trajectory will repeatably generate the desired forces in the suit.

4.3 Actuator system performance during walking: Forces and Power

4.3.1 Forces

Data was collected on the performance of the actuation system. Figure 9(a) shows the trapezoidal position trajectory, the smoothed position trajectory, and the resulting force in the suit for a subject walking at 1.25m/s (2.8mph). The force profile increases passively from 20-40% in the gait cycle due to the body's motion, and then it ramps upward sharply when the actuation begins. This

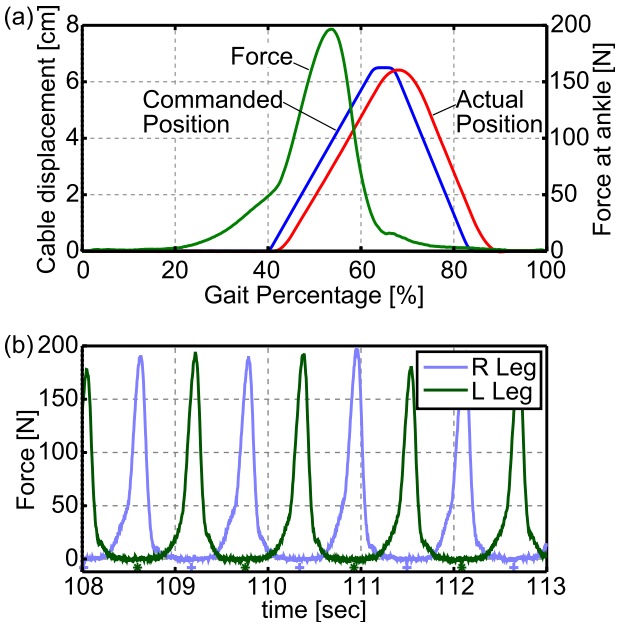

Figure 9: (a) Plot showing the trapezoidal position sent to the motor controller, the smoothed actual position of the cable, and the resulting force in the suit. With the position curves, positive values correspond to retracting the cable and shortening the suit. (b) Plot showing the pattern of force in the suit over time for both legs, with heelstrikes indicated at the bottom by $+$ symbols for the right leg and $*$ symbols for the left leg.

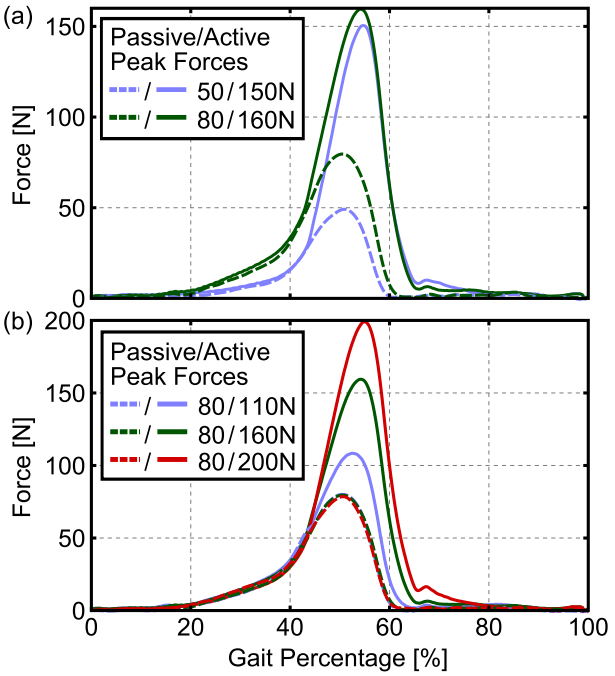

Figure 10: (a) Plot showing changes in the force profile resulting from two different initial unstretched suit lengths. In the two conditions, the initial unstretched suit length was set so that the peak passive force was 50N or 80N, respectively. Then, the same cable actuation profile was applied to shorten the unstretched suit length, which resulted in different active force profiles with peaks of 150N and 160N, respectively. (b) In this plot, the initial unstretched suit length was held the same in all conditions, resulting in a peak passive force of 80N. The pull amplitudes were varied, which resulted in peak forces of 110N, 160N, and 200N for actuation amplitudes of 1.5cm, 4.0cm, and 6.0cm, respectively.

profile, including components due to both passive tensioning and active contraction, is similar to the nominal biological moments at the ankle and hip shown previously in Figure 2. While not a perfect match, this indicates that the motor profiles used in the system can generate biologically-appropriate forces.

Figure 9(b) shows the forces in the right and left legs over time, with footstrikes indicated below. As shown here, the peak force during each step varied slightly over time, due primarily to the subject's varying their cadence. In addition, with the control scheme estimating the current gait period based on the past five steps, if the current step is different than that average, the timing and hence forces will be slightly off. In one example trial with a mean peak force of 195.6N, the actual peak forces ranged from 150.0-234.1N with a standard deviation of 19.8N.

Due to our control scheme altering the unstretched suit length with a position-controlled profile, the shape of the resulting force pulse will vary as a function of the initial unstretched suit length and the pull amplitude. Figure 10(a) shows how changing the initial unstretched suit length leads to a different shape of the force profile at 20-50% in the gait cycle. In the figure, the initial suit length was adjusted so that the peak passive forces were 50N and 80N for the two conditions shown, and then the same actuation profile was applied in each case to give the force curves in the figure. The higher passive force results in almost double the power absorbed by the suit between 20-40% in the gait cycle. Furthermore, when the suit is actuated, the peak force (at 55% in the gait cycle) is higher. This is because the suit has additional force in it already when the actuation begins.

Conversely, Figure 10(b) illustrates how increasing the motor pull amplitude changes the peak force as well as changing the shape of the force profile when it is falling. This is due to the actual motor position trajectory being slightly different for the different amplitudes, since the motor and controller cannot follow the desired profiles exactly. Ideally the forces would all drop to zero at around 63% in the gait cycle, which is when the ankle biological moment drops to zero, but the motor is too slow to return to zero quickly enough for higher pull amplitudes. The positive force after this point absorbs power from the body, which is counterproductive.

4.3.2 Power transfer

Figure 11(a) shows the power at various stages in the actuation system with a subject walking at 1.25m/s and with a peak suit force of 188N. The input electrical power is

computed from the current and voltage sent to the motor, reported by the motor controller. The mechanical power at the output of the gearbox is computed using the motor speed and the cable force in the pulley module, while the mechanical output at the ankle is computed using the motor speed and force at the ankle. Each leg uses 21.8W of input electrical power on average, and 6.6W of power are delivered to the bottom of the Bowden cable. The Bowden cable in this trial was a new cable that had an average efficiency of 74.7%, as compared to a worn cable which has an efficiency of 50-60%.

Figure 11(b) shows the power flow between the suit and the human. The power is input to the suit from the bottom of the Bowden cable, shown in the graph as ("Cable Output") which is repeated from part (a) of the figure. The suit stretches from 20-55% in the gait cycle and then springs back after this point, returning approximately 65% of the energy to the wearer as determined by the suit-human stiffness experiments. We compute the power absorbed and returned by the suit by using the force in the suit and the suit-human series stiffness model. Given the force at the ankle, we use the inverse of the stiffness model to compute x_{taut}, which is the length discrepancy that must be accommodated by the body's compressing and the suit's stretching. We then take the time-derivative of x_{taut} and multiply it by the force in the suit to compute the suit power; this is plotted in the graph as "Suit-Calc." The suit power is positive until 55% in the gait cycle, which corresponds to its absorbing power from the human and motor. The suit then retracts, returning power to the human, which is shown as a negative value. In this trial, the force became non-zero at only 35% in the gait cycle, as compared to typically closer to 20%, which is why the suit power is zero until that point.

We then can calculate the power delivered to the human by taking the difference between the power input to the suit from the Bowden cable ("Cable Output") and the computed suit power ("Suit-Calc."), since the power input to the suit must either go into the suit or the human, and the hysteresis losses are already included in the suit power. The result ("Human-Calc.") is negative until 50% in the gait cycle, corresponding to power being absorbed from the human, and then is positive after that. This power transferred to/from the human is the sum of the powers delivered to the ankle, hip, and knee.

In addition to calculating the power delivered to the human via the suit-human series stiffness model, we measured the power delivered to the human through a different method. We used a Vicon motion tracking system to determine the joint velocities of the ankle, knee, and hip as well as the moment arms between the suit and the biological joints. We compute the measured power by combining these quantities with the measured force in the suit and sum them to get the "Human-Meas." curve in the figure, assuming that the force in the suit is equal across all three joints. This measured power is 12% different than the

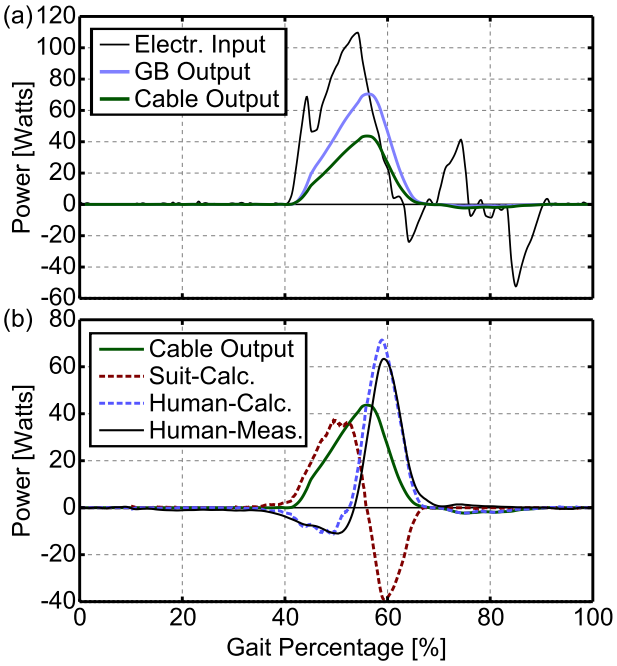

Figure 11: (a) Plot showing the instantaneous power at various locations along the transmission: "Electr. Input" is the input electrical power to the motor, "GB Output" is the mechanical power at the output of the gearbox, and "Cable Output" is the mechanical power at the bottom of the Bowden cable. (b) Plot showing several curves explaining how the power is transferred from the cable to the wearer. The "Cable Output" curve is repeated from the top graph. The "Suit-Calc." curve shows the power absorbed and released by the suit, based on the suit-human series stiffness model. Positive values mean that power is absorbed by the suit and negative values mean that the suit is returning the power. The "Human-Calc." curve is the resulting power delivered to the wearer through the suit, also estimated based on the suit-human series stiffness model. For comparison, the "Human-Meas." curve is the measured power delivered to the human based on the force at the ankle of the suit, the moment arms from the suit to each of the ankle, knee, and hip, and the angular velocities of these joints. In calculating this we assume the force in the suit is equal across all three joints. Positive values mean that power is transmitted to the human, and negative values mean that power is absorbed from the human.

power estimated by the suit-human series stiffness model, a close match. The discrepancy may be due to a variety of factors, including a difference between the suit's fit on the subject and that assumed by the model, which is based on the average of many subjects; there may be errors in the measured moment arms or joint velocities; and the force in the suit at the hip is likely less than it is at the ankle due to the suit's applying pressure to the body along the entire leg.

5 Biomechanical and Physiological Results

To evaluate the effect of the exosuit on the wearer's gait kinematics and energetics, and to determine the force and power delivered to the human, the system was tested on a group of $N = 5$ healthy young subjects with no gait abnormalities. Subjects' age ($\pm$ SD) was 25.2 ± 3.9, height was 183.8 ± 6.1cm and weight 85.6 ± 12.1kg. Experiments were approved by the Harvard IRB, and subjects participated in the study after written consent.

5.1 Materials and Methods

Experiments were conducted at the Wyss Motion Capture Laboratory. Subjects walked on a Bertec FIT instrumented split-belt treadmill (Bertec Corporation, Columbus, OH) at a speed of 1.25m/s. A Vicon T-Series 9-camera system (Vicon Motion Systems Ltd., Oxford, UK) was used for motion tracking. To measure metabolic expenditure, a COSMED K4b2 breath-by-breath, portable pulmonary gas exchange measurement system (COSMED Srl, Rome, Italy) was worn by the subject.

The subjects wore an additional load in order to simulate hiking scenarios. The carried mass included the exosuit and actuation system (10.1kg) mounted on a MOLLE external frame backpack (3.7kg) that was filled with 19.3kg of weight. Subjects also wore a COSMED system (1.5kg) for a total carried mass of 34.6kg. Subjects experience in wearing exosuit systems varied from completely naïve (four subjects) to very experienced (one subject).

The experimental protocol involved multiple 8-minute walking sessions interleaved by 5 minutes of sitting rest. Before the protocol took place, a 20 minute warm-up walking session was performed to acclimate the subjects to the experimental setup and to the exosuit, during which time the suit was active for approximately 10 minutes.

The protocol was a proof-of-concept study designed to determine the gross benefit (device active vs. device worn but not active) of the exosuit on the wearer, since the actuation units were not optimized for weight. Measuring the gross benefit of the system allows the impact of the assistive forces to be determined; this can be used to predict the net benefit given different system masses. As such, the protocol involved a "slack" condition, in which the suit and system were worn but the cable length was set loosely so the suit applied no force to the wearer, and "active" conditions, in which the exosuit was actively applying forces during walking. Each 8-minute session involved a single condition, and the "slack" condition was tested at the beginning and end of the protocol. For the middle conditions, multiple passive peak force and active peak force combinations were tested (passive peak: 50N, 80N; active peak: 100N, 150N, 200N).

In the remainder of this section, the notation of X/Y N will indicate an "active" condition with a passive peak of X N and an active peak of Y N. During walking in passive mode, the peak forces were set to X N by adjusting the initial unstretched suit length. Once the actuation was turned on, the actuation pull amplitude was set so that the peak force was Y N.

Gait kinematics were evaluated for $N = 1$ subject through a full-body 53-marker set based on the modified Cleveland Clinic marker set. Inverse kinematics was performed to reconstruct joint angles in the sagittal plane using Visual3D (C-Motion Inc., Germantown, MD) and custom scripts written in MATLAB r2013a (The Mathworks Inc., Natick, MA). Gait variables were measured over a 1-minute window at the end of each 8-minute session.

The metabolic cost of walking was evaluated by measuring the O_2 and CO_2 gas exchanges between the subject and the environment. Data was filtered through a 2-minute moving average. The (normalized) metabolic cost of walking was estimated by applying Brockway's standard equations (Brockway, 1987) and by selecting a steady-state window at the end of the 8-minute session (defined as having less than 3% peak-peak variability).

5.2 Results

5.2.1 Biomechanical results: Kinematic and gait changes

Figure 12 shows the kinematics for one subject during several actuation conditions. For these initial results, the knee and hip trajectories during the "active" conditions were less than 2° different than those in the "slack" conditions throughout the gait cycle. During the "active" conditions, the ankle trajectories were shifted towards plantarflexion (toe pointing down) throughout the gait cycle, with differences of up to 3° with respect to the "slack" conditions at the peak dorsiflexion angle.

For all subjects, we did not find a significant difference in step length, step width, and stance time (as measured by the force-sensing treadmill) in all the "active" relative to "slack" conditions.

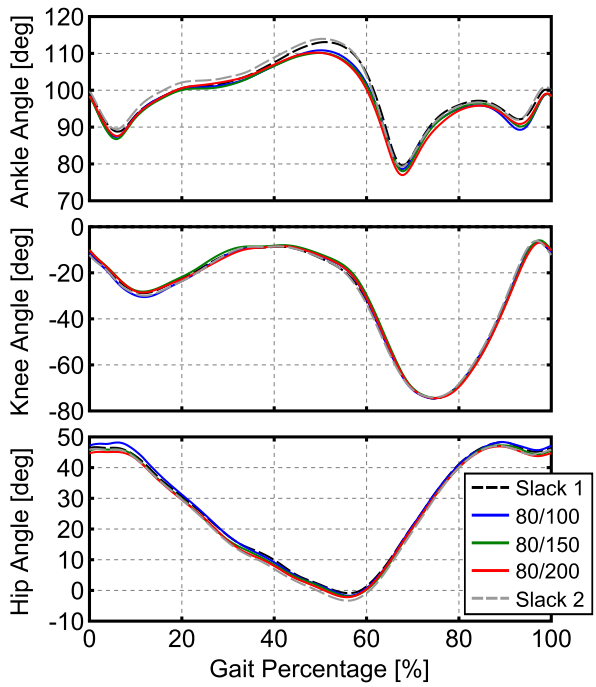

Figure 12: Effect of the exosuit on gait kinematics, shown for one subject. Top to bottom, ankle, knee and hip angles in the sagittal plane. Five conditions are shown, corresponding to the two "slack" conditions (Slack 1: before active conditons, Slack 2: after active conditions) and three "active" conditions with different peak forces (80/100, 80/150, 80/200).

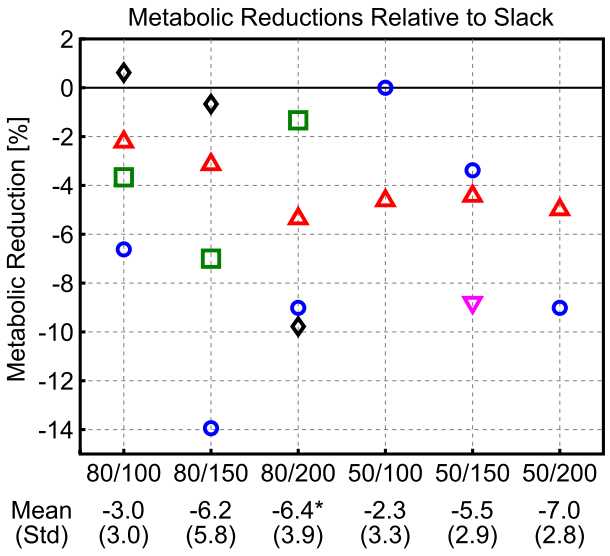

Figure 13: Summary of metabolic reductions in testing, comparing the "active" conditions vs. the "slack" condition. A negative reduction corresponds to energy saving. Each subject is a different symbol, and each subject performed a subset of all possible conditions. The average metabolic reductions are shown below each condition, with an asterisk indicating that the result is significantly different than zero, $p < 0.05$.

5.2.2 Metabolic results

In all the test sessions, steady-state metabolic cost during the two slack conditions (before and after the active trials) were nearly identical (<1% difference), indicating that fatigue or other base variations in metabolic rate did not occur over the course of the experiment.

Figure 13 shows results from metabolic testing of the system, comparing the metabolic cost of walking in the various conditions. As previously mentioned, different passive and active peak forces were used. As shown in the plot, two subjects performed all six possible test conditions, while three subjects performed only a subset of the possible conditions.

The average metabolic reduction for the 80/200 condition was -6.4% $\pm$ 3.9%; this was the best-performing condition tested on four subjects. This corresponded to a metabolic power reduction of 36W ("slack"= 575W, "active"= 539W). This was the only condition that had a statistically significant reduction as compared to zero ($p < 0.05$). Combining the results from all subjects and all conditions, the average metabolic reduction was -5.1% $\pm$ 3.8%, which was statistically significant ($p < 5e-5$).

5.3 Discussion

Our initial results suggest that the exosuit does not grossly change the wearer's gait when active as compared to slack, appearing to affect mostly the ankle angle which is shifted toward plantarflexion throughout the gait cycle, and primarily between 40-65% in the gait cycle when the suit is actuated. Thus, the device does not appear to drastically disrupt normal walking biomechanics.

It makes sense that the ankle trajectories should be shifted toward plantarflexion, because the suit pulls up on the back of the heel for approximately a third of the gait cycle. Interestingly, Silder et al. (2013) show that during load carriage, the peak ankle dorsiflexion angles increased with load; if these initial kinematic results are true for other subjects, our system would move the ankle angle in a direction to undo this.

Interestingly, the suit appeared to function similarly on expert and naïve subjects. The expert subject (upward-pointing triangles in Figure 13) did not achieve a larger metabolic reduction than the naïve subjects, indicating that likely the naïve subjects had adapted well to the system within the 20-minute warm-up period.

Preliminary experiments were performed in which the metabolic cost of carrying the system mass was quantified. It was found to raise the metabolism 16-17.5%, which is about 1.55%/kg of system mass (10.1kg), a value between 1-2%/kg which is for mass carried on the torso, and 8%/kg for mass at the foot (Browning et al, 2007). As such, considering the 80/200 condition, it can be esti-

mated that the system resulted in a net metabolic increase of 9.3%. Assuming a 6.4% gross metabolic benefit (with the 80/200 condition), this first generation system applying the assistance levels reported in this paper would have to be less than 4.4kg to create a net metabolic savings. At this break-even point, the system could be worn for long periods of time for rehabilitation without burdening the wearer with a heavy payload. An even lighter device could achieve the goal of assisting human locomotion by saving the wearer energy. The current system achieved the design goal of minimizing distal mass, with only 2.0kg (20% of total system mass) worn on the legs.

Qualitatively, subjects found the suit to be comfortable. The long-term effects of wearing the suit (>4 hours) still need to be investigated. In our experiments, subjects wore the suit continuously for 3-4 hours, although they were only walking for a maximum of 30-50% of this time. When the suit is active, the bottom of the upper suit does move around 2cm downward over the calf as actuation is applied, but this motion did not lead to chafing or discomfort.

6 Conclusions and future work

In this paper, we have presented the design and evaluation of a first generation multi-articular soft exosuit that is portable, fully autonomous, and provides assistive torques to the wearer at the ankle and hip during walking. In addition to presenting design details and performance specifications, we demonstrated that such a system can decrease the gross metabolic cost of walking (comparing suit powered vs. worn and unpowered) with minimal restrictions to the wearers natural gait. Having achieved this exciting proof-of-concept, we have now identified a number of areas for technical improvements and a feasible path forward to achieving a net metabolic benefit. As was discussed, due to the current actuation system, the cable speed is limited and on occasions some power can be absorbed from the wearer at around 70% in the gait cycle (i.e. during the swing phase) which negatively impacts the metabolic effort. This will be addressed through an optimized actuation transmission in future system revisions. Our current suit is made of individual webbing straps that are prone to migrating on the body during use. Transitioning to solid pieces of fabric with carefully tailored properties will increase the surface area, limit migration and improve the suit-human series stiffness. The foot switches, which are relatively heavy and not robust, could be eliminated with the use of other sensors such as inertial measurement units or gyroscopes. The volume and mass of the current actuator units that are mounted on the sides of a backpack can also be greatly reduced to make them more unobtrusive and easier to carry.

In addition to the abovementioned technical improvements, there is much basic research to be undertaken in the area of human-machine interaction with soft exosuits. In particular, the field will need to understand 1) how to apply larger forces through a soft textile interface and how this impacts the underlying musculoskeletal system, and 2) how to design controllers that provide synergistic interaction between the wearer and the device. In terms of increasing forces, a challenge may be how the joints of the wearer are loaded in compression, since there is no external skeleton. However, if the muscles adapt to the assistance and thus decrease their activation and generated force to maintain the same total (exosuit plus wearer) joint torques, the total force on the bones should remain constant or even decrease. This would occur because the suit has a larger moment arm with which to apply joint torques than do the muscles, so smaller forces are required to achieve the same torques. However, the peak suit force will be limited by the maximum pressure the skin and underlying tissue can support in conjunction with the available surface area through which force can be transferred to the waist and leg. With regards to improved controllers, our work to date has shown how sensitive a wearer is to small levels of assistance and thus methods are required to ensure reliable detection of user action and intent, both across subjects and a variety of different gaits and terrains.

In the future, we also envision exosuits being worn by individuals undergoing rehabilitation as well as the elderly, soldiers, and recreational users. The devices could be worn under the clothing and be unobtrusive. For these applications, further work must also be done to determine the best control strategies and assistive force profiles. The multi-articular architecture described here will be useful so long as torques can be provided to ankle plantarflexion and hip flexion simultaneously. Future designs will have better energy return and stiffness properties (guided by modeling to understanding how forces are generated in the suit), and will enable the devices to be worn in passive modes, potentially providing benefit to the wearer with no applied actuation.

Acknowledgements

This material is based upon work supported by the Defense Advanced Research Projects Agency (DARPA), Warrior Web Program (Contract No. W911QX-12-C-0084). The views and conclusions contained in this document are those of the authors and should not be interpreted as representing the official policies, either expressly or implied, of DARPA or the U.S. Government.

The authors would like to thank Robert J. Dyer and Michael Mogenson for their help with construction of the actuation units, and Arnar F. Larusson for his help with the exosuit design, construction, and stiffness testing. The authors would also like to thank Hao Pei, Ye Ding and Patrick Aubin for their help with human subjects testing and data processing.

References

Ackerman E (2010) Berkeley bionics introduces eLEGS robotic exoskeleton. IEEE Spectrum 10

Asbeck AT, Dyer R, Larusson A, Walsh CJ (2013) Biologically-inspired soft exosuit. In: Rehabilitation Robotics (ICORR), 2013 IEEE International Conference on, IEEE

Banala S, Agrawal S, Scholz J (2007) Active leg exoskeleton (ALEX) for gait rehabilitation of motor-impaired patients. In: Rehabilitation Robotics, 2007. ICORR 2007. IEEE 10th International Conference on, IEEE, pp 401–407

Belanger M, Patla AE (1984) Corrective responses to perturbation applied during walking in humans. Neuroscience letters 49(3):291–295

Brockway JM (1987) Derivation of formulae used to calculate energy expenditure in man. Human nutrition Clinical nutrition 41(6):463–71

Browning RC, Modica JR, Kram R, Goswami A, et al (2007) The effects of adding mass to the legs on the energetics and biomechanics of walking. Medicine and science in sports and exercise 39(3):515

Cempini M, De Rossi SMM, Lenzi T, Vitiello N, Carrozza MC (2013) Self-alignment mechanisms for assistive wearable robots: A kinetostatic compatibility method

Collins S, Ruina A, Tedrake R, Wisse M (2005) Efficient bipedal robots based on passive-dynamic walkers. Science 307(5712):1082–1085

Cool J (1989) Biomechanics of orthoses for the subluxed shoulder. Prosthetics and Orthotics international 13(2):90–96

Doke J, Donelan JM, Kuo AD (2005) Mechanics and energetics of swinging the human leg. The Journal of Experimental Biology 208(3):439–445

Dollar A, Herr H (2008) Lower extremity exoskeletons and active orthoses: Challenges and state-of-the-art. Robotics, IEEE Transactions on 24(1):144–158

Donelan JM, Kram R, Kuo AD (2002) Mechanical work for step-to-step transitions is a major determinant of the metabolic cost of human walking. Journal of Experimental Biology 205(23):3717–3727

Ergin MA, Patoglu V (2011) A self-adjusting knee exoskeleton for robot-assisted treatment of knee injuries. In: Intelligent Robots and Systems (IROS), 2011 IEEE/RSJ International Conference on, IEEE, pp 4917–4922

Esquenazi A, Talaty M, Packel A, Saulino M (2012) The ReWalk powered exoskeleton to restore ambulatory function to individuals with thoracic-level motor-complete spinal cord injury. American Journal of Physical Medicine & Rehabilitation 91(11):911–921

Ferris D, Lewis C (2009) Robotic lower limb exoskeletons using proportional myoelectric control. In: Engineering in Medicine and Biology Society, 2009. EMBC 2009. Annual International Conference of the IEEE, IEEE, pp 2119–2124

Finni T, Peltonen J, Stenroth L, Cronin NJ (2013) Viewpoint: On the hysteresis in the human achilles tendon. Journal of Applied Physiology 114(4):515–517

Gams A, Petric T, Debevec T, Babic J (2013) Effects of robotic knee exoskeleton on human energy expenditure. IEEE Trans Biomed Engineering 60(6):1636–1644

Garcia E, Sater JM, Main J (2002) Exoskeletons for human performance augmentation (EHPA): A program summary. Journal-Robotics Society Of Japan 20(8):44–48

Grabowski AM, Herr HM (2009) Leg exoskeleton reduces the metabolic cost of human hopping. Journal of Applied Physiology 107(3):670–678

Gregorczyk K, Obusek J, Hasselquist L, Bensel J, Carolyn K, Gutekunst D, Frykman P (2006) The effects of a lower body exoskeleton load carriage assistive device on oxygen consumption and kinematics during walking with loads. Tech. rep., DTIC Document

Helbostad JL, Leirfall S, Moe-Nilssen R, Sletvold O (2007) Physical fatigue affects gait characteristics in older persons. The Journals of Gerontology Series A: Biological Sciences and Medical Sciences 62(9):1010–1015

Herr H (2009) Exoskeletons and orthoses: classification, design challenges and future directions. Journal of NeuroEngineering and rehabilitation 6:21

Hidler JM, Wall AE (2005) Alterations in muscle activation patterns during robotic-assisted walking. Clinical Biomechanics 20(2):184–193

Hollander KW, Sugar TG (2007) Powered human gait assistance. Rehabilitation robotics pp 203–219

Hollander KW, Ilg R, Sugar TG, Herring D (2006) An efficient robotic tendon for gait assistance. Journal of biomechanical engineering 128:788

Holloway G, Daly C, Kennedy D, Chimoskey J (1976) Effects of external pressure loading on human skin blood flow measured by 133xe clearance. Journal of Applied Physiology 40(4):597–600

Imamura Y, Tanaka T, Suzuki Y, Takizawa K, Yamanaka M (2011) Motion-based design of elastic belts for passive assistive device using musculoskeletal model. In: Robotics and Biomimetics (ROBIO), 2011 IEEE International Conference on, IEEE, pp 1343–1348

In H, Cho KJ, Kim K, Lee B (2011) Jointless structure and under-actuation mechanism for compact hand exoskeleton. In: Rehabilitation Robotics (ICORR), 2011 IEEE International Conference on, IEEE, pp 1–6

Jezernik S, Colombo G, Keller T, Frueh H, Morari M (2003) Robotic orthosis Lokomat: a rehabilitation and research tool. Neuromodulation: Technology at the Neural Interface 6(2):108–115

Kang BB, In H, Cho K (2012) Force transmission in jointless tendon driven wearable robotic hand. In: Control, Automation and Systems (ICCAS), 2012 12th International Conference on, IEEE, pp 1853–1858

Kawamoto H, Lee S, Kanbe S, Sankai Y (2003) Power assist method for HAL-3 using emg-based feedback controller. In: Systems, Man and Cybernetics, 2003. IEEE International Conference on, IEEE, vol 2, pp 1648–1653

Kawamura T, Takanaka K, Nakamura T, Osumi H (2013) Development of an orthosis for walking assistance using pneumatic artificial muscle: A quantitative assessment of the effect of assistance. In: Rehabilitation Robotics (ICORR), 2013 IEEE International Conference on, IEEE, pp 1–6

Kazerooni H, Steger R (2006) The Berkeley Lower Extremity Exoskeleton. Journal of Dynamic Systems, Measurement, and Control 128:14–25

Kobayashi H (2002) New robot technology concept applicable to human physical support-the concept and possibility of the muscle suit (wearable muscular support apparatus). J Robotics Mechatron 14(1):46–53

Malcolm P, Derave W, Galle S, De Clercq D (2013) A simple exoskeleton that assists plantarflexion can reduce the metabolic cost of human walking. PloS One 8(2):e56,137

McGeer T (1990) Passive dynamic walking. The International Journal of Robotics Research 9(2):62–82

Mizrahi J, Verbitsky O, Isakov E, Daily D (2000) Effect of fatigue on leg kinematics and impact acceleration in long distance running. Human movement science 19(2):139–151

Mooney LM, Rouse EJ, Herr HM (2014) Autonomous exoskeleton reduces metabolic cost of human walking during load carriage. Journal of NeuroEngineering and Rehabilitation 11(1):80

Neuhaus PD, Noorden JH, Craig TJ, Torres T, Kirschbaum J, Pratt JE (2011) Design and evaluation of Mina: A robotic orthosis for paraplegics. In: Rehabilitation Robotics (ICORR), 2011 IEEE International Conference on, IEEE, pp 1–8

Ohta Y, Yano H, Suzuki R, Yoshida M, Kawashima N, Nakazawa K (2007) A two-degree-of-freedom motor-powered gait orthosis for spinal cord injury patients. Proceedings of the Institution of Mechanical Engineers, Part H: Journal of Engineering in Medicine 221(6):629–639

Park YL, Chen Br, Young D, Stirling L, Wood RJ, Goldfield E, Nagpal R (2011) Bio-inspired active soft orthotic device for ankle foot pathologies. In: Intelligent Robots and Systems (IROS), 2011 IEEE/RSJ International Conference on, IEEE, pp 4488–4495

Perry J, Burnfield J (2010) Gait analysis: normal and pathological function, 2nd edn. SLACK Incorporated

Pohl MB, Rabbito M, Ferber R (2010) The role of tibialis posterior fatigue on foot kinematics during walking. Journal of Foot and Ankle Research 3(1):1–8

Pons JL (2010) Rehabilitation exoskeletal robotics. Engineering in Medicine and Biology Magazine, IEEE 29(3):57–63

Pratt J, Krupp B, Morse C, Collins S (2004) The RoboKnee: an exoskeleton for enhancing strength and endurance during walking. In: Robotics and Automation, 2004. Proceedings. ICRA'04. 2004 IEEE International Conference on, IEEE, vol 3, pp 2430–2435

Quintero H, Farris R, Goldfarb M (2011) Control and implementation of a powered lower limb orthosis to aid walking in paraplegic individuals. In: Rehabilitation Robotics (ICORR), 2011 IEEE International Conference on, IEEE, pp 1–6

Rose J, Gamble JG (2006) Human walking. Lippincott Williams & Wilkins Philadelphia

Sawicki GS, Ferris DP (2009a) A pneumatically powered knee-ankle-foot orthosis (KAFO) with myoelectric activation and inhibition. Journal of neuroengineering and rehabilitation 6(1):23

Sawicki GS, Ferris DP (2009b) Powered ankle exoskeletons reveal the metabolic cost of plantar flexor mechanical work during walking with longer steps at constant step frequency. Journal of Experimental Biology 212(1):21–31

Schiele A (2009) Ergonomics of exoskeletons: Objective performance metrics. In: EuroHaptics conference, 2009 and Symposium on Haptic Interfaces for Virtual Environment and Teleoperator Systems. World Haptics 2009. Third Joint, IEEE, pp 103–108

Schiele A, van der Helm FC (2009) Influence of attachment pressure and kinematic configuration on phri with wearable robots. Applied Bionics and Biomechanics 6(2):157–173

Shadwick RE (1990) Elastic energy storage in tendons: mechanical differences related to function and age. J Appl Physiol 68(3):1033–1040

Shorter KA, Kogler GF, Loth E, Durfee WK, Hsiao-Wecksler ET (2011) A portable powered ankle-foot orthosis for rehabilitation. Journal of Rehabilitation Research & Development 48(4):459–472

Silder A, Delp SL, Besier T (2013) Men and women adopt similar walking mechanics and muscle activation patterns during load carriage. Journal of Biomechanics 46(14):2522–2528

Stirling L, Yu CH, Miller J, Hawkes E, Wood R, Goldfield E, Nagpal R (2011) Applicability of shape memory alloy wire for an active, soft orthotic. Journal of materials engineering and performance 20(4-5):658–662

Strausser K, Kazerooni H (2011) The development and testing of a human machine interface for a mobile medical exoskeleton. In: Intelligent Robots and Systems (IROS), 2011 IEEE/RSJ International Conference on, IEEE, pp 4911–4916

Tanaka T, Satoh Y, Kaneko S, Suzuki Y, Sakamoto N, Seki S (2008) Smart suit: Soft power suit with semi-active assist mechanism-prototype for supporting waist and knee joint. In: Control, Automation and Systems, 2008. ICCAS 2008. International Conference on, IEEE, pp 2002–2005

Tang PF, Woollacott MH, Chong RK (1998) Control of reactive balance adjustments in perturbed human walking: roles of proximal and distal postural muscle activity. Experimental Brain Research 119(2):141–152

Vanoglio F, Luisa A, Garofali F, Mora C (2013) Evaluation of the effectiveness of Gloreha (Hand Rehabilitation Glove) on hemiplegic patients. Pilot study. In: XIII Congress of Italian Society of Neurorehabilitation

Veneman J, Kruidhof R, Hekman E, Ekkelenkamp R, Van Asseldonk E, van der Kooij H (2007) Design and evaluation of the LOPES exoskeleton robot for interactive gait rehabilitation. Neural Systems and Rehabilitation Engineering, IEEE Transactions on 15(3):379–386

Walsh C, Endo K, Herr H (2007) A quasi-passive leg exoskeleton for load-carrying augmentation. International Journal of Humanoid Robotics 4(03):487–506

Wehner M, Rempel D, Kazerooni H (2009) Lower extremity exoskeleton reduces back forces in lifting. In: ASME 2009 Dynamic Systems and Control Conference, American Society of Mechanical Engineers, pp 49–56

Wehner M, Quinlivan B, Aubin PM, Martinez-Villalpando E, Baumann M, Stirling L, Holt K, Wood R, Walsh C (2013) A lightweight soft exosuit for gait assistance. In: Robotics and Automation (ICRA), 2013 IEEE International Conference on, IEEE, pp 3362–3369

Yamamoto K, Ishii M, Hyodo K, Yoshimitsu T, Matsuo T (2003) Development of power assisting suit (miniaturization of supply system to realize wearable suit). JSME International Journal Series C 46(3):923–930